SLAC–PUB–4376
UM–HE–87–18
LBL–23819
August 1987
(T/E)

RADIATIVE CORRECTIONS TO THE Z^0 RESONANCE*

JAMES P. ALEXANDER, GIOVANNI BONVICINI,
PERSIS S. DRELL, AND RAY FREY

Lawrence Berkeley Laboratory, Berkeley, CA 94720

University of Michigan, Ann Arbor, MI 48109

Stanford Linear Accelerator Center, Stanford University, Stanford, CA 94305

ABSTRACT

We review calculations of the radiative corrections to the Z^0 resonance, and we show that while the radiative corrections are quite large, they can be calculated and incorporated into the comparison with experiment so that there will be no significant theoretical uncertainties on the measurements of the Z^0 mass and width at SLC and LEP. We compare calculations based on matrix elements and structure function methods, and discuss two Monte Carlo's based on these calculations. We use the new calculations to refit the J/ψ resonance.

Submitted to *Physical Review D*

* Work supported by the Department of Energy, Contracts DE–AC03–76SF00515 (SLAC), DE–AC03–76SF00098 (LBL) and DE–AC02–84ER40125 (U. of Mich.).

The experimental evidence supporting the standard model of electroweak interactions is impressive. Perhaps most spectacular of all has been the direct observation of the Z^0, the heavy gauge boson predicted by the model, at the $p\bar{p}$ collider at CERN. Once one can directly produce Z^0s, one is in an excellent position to do detailed studies of the electroweak interaction, both by studying in Z^0 decays how the Z^0 couples to the matter fields of quarks and leptons, and by precision measurements of the resonance itself.

The Z^0 resonance, in lowest order, has a Breit–Wigner line shape which is characterized by experimentally measurable quantities: the peak position or mass, the width, and the peak cross section. From an experimental point of view the three parameters, mass, width, and cross section, are independent quantities to be determined. Within the context of the standard model, however, they take on deeper significance that both motivates their measurement and sets the scale of precision at which the measurements may be considered interesting. The mass is related to $\sin^2\theta_W$; the width depends on the number of particles of mass less than half the mass of the Z^0 which couple to the Z^0; and the peak cross section is related to the vector and axial vector couplings, and hence $\sin^2\theta_W$.

Precision studies of the Z^0 resonance have not been forthcoming from the $Sp\bar{p}S$ where the Z^0 was first discovered. The broad spectrum of parton energies in $p\bar{p}$ collisions means that only a small portion of the total luminosity manifests itself in production of the relatively narrow Z^0 peak, and the resonance is difficult to extract from the much larger nonresonant QCD background. In the exclusive leptonic decay modes of the Z^0, which have clean signatures and can be easily extracted from the background events, the mass of the Z^0 can only be determined from the invariant mass of the lepton pair, since the initial state energy is unknown.

At the SLC and LEP, the situation is quite different. Because the electron and positron are pointlike, the center-of-mass energy of the interaction is defined by the beam energy. The beam energy spread is small compared to the resonance

width, and all the luminosity contributes to the signal. The background is small and all visible decay modes of the Z^0 can be used.

Since it is the beam energy which will be used to determine the mass and width of the Z^0, it is crucial to know the absolute beam energy and energy spread. For the Mark II at SLC, a pair of spectrometers[1] located just upstream of the beam dumps will measure the central value of the beam energies to ± 30 MeV, and will provide information on the beam energy spread, expected to be about 100 MeV. Systematic errors on the mass and width of the Z^0 are expected to be around ± 45 MeV. The measurement of the peak cross section of the resonance will be limited by systematic errors in the monitoring of the machine luminosity. The luminosity monitors[2] measure the reaction $e^+e^- \rightarrow e^+e^-$ at small angles where it is dominated by the QED t-channel scattering. In this steeply falling region of the cross section the acceptance determination dominates the systematic error, which is not expected to be better than $\sim 2\%$ overall. Long-term stability should be much better, and point-to-point variations in an energy scan will be low.

The Z^0 resonance is profoundly altered from its zeroth order Breit–Wigner shape by radiative corrections. In particular, bremsstrahlung from the annihilating e^+ and e^- alters the effective center-of-mass energy and significantly changes any quantity that varies strongly with $\sqrt{s}$. This results in shifts of hundreds of MeV in the peak position and width of the resonance, and lowers the peak cross section by tens of percent. This paper will review in detail the physics of these corrections, the existing calculations, available Monte Carlos, and the level of precision finally expected in radiative corrections to Z^0 line shape measurements. Since we will have excellent energy resolution for the Z^0 mass and width measurement but cruder luminosity monitoring for the cross section measurement, radiative corrections which affect the line shape and peak position must be quite carefully considered, while corrections to the overall normalization at or below the 1% level are less urgent. In particular, the radiative corrections to the Z^0 are overwhelmingly dominated by initial state QED effects. Recent

work extending the calculations to second order has given confidence that QED radiative corrections are well understood and that the precision achievable in these corrections is significantly better than the 45 MeV currently expected to limit experimental measurements. For the precision measurements of the mass and width of the Z^0 at SLC and LEP, we demonstrate that all calculations that include exponentiation of the soft photons and virtual corrections to at least first order are adequate. Detailed calculations of electroweak radiative corrections are unnecessary for these measurements since they only modify the relationship between the peak cross section and the mass of the Z^0, and do so at a level level that is unobservable given the experimental uncertainties in the luminosity.

In Sec. 1 we will review radiative corrections to first order. Results will be extended to higher orders in Sec. 2, and we will discuss, quantitatively, the necessary accuracy of the calculations. The third section will present the radiative corrections from a structure function point of view. The advantages of this method will be discussed, and in Sec. 4 we will present a numerical comparison of all the available calculations, with the conclusion that the agreements and disagreements between the different calculations are well understood, and the theoretical uncertainties are well below the anticipated experimental systematic errors. Section 5 will discuss currently available MC event generators, and in Sec. 6 we will use the new calculations to refit the J/ψ resonance which will increase the measured leptonic width of the resonance by one standard deviation compared to the current world average.

1. QED Radiative Corrections to First Order

In lowest order, $e^+e^- \to f\bar{f}$ proceeds by photon exchange and by Z^0 exchange as shown in Fig. 1. The total cross section is given in the standard model by

$$\sigma_0(s) = \frac{4\pi\alpha^2}{3s} N \left[Q^2 - \frac{2s(s-M_Z^2)\rho M_Z^2 Q v_e v_f}{(s-M_Z^2)^2 + s\Gamma_Z^2} + \frac{s^2\rho^2 M_Z^4 (v_e^2+a_e^2)(v_f^2+a_f^2)}{(s-M_Z^2)^2 + s\Gamma_Z^2} \right] \tag{1}$$

where

$$\rho = \frac{G_F}{2\sqrt{2}\pi\alpha} \quad , \tag{2}$$

and the vector and axial vector coupling strengths for the electron and for the final fermion are

$$v = -1/2 + 2Q\sin^2\theta_W, \quad a = -1/2 \quad . \tag{3}$$

N and Q denote the number of colors and charge of the fermion. At SLC energies, the first two terms in Eq. (1), the QED and interference contributions, are negligible compared to the third, resonant term. To an excellent approximation one writes the lowest order cross section $\sigma_0(s)$ as

$$\sigma_0(s) = \sigma_Z \frac{s\Gamma_Z^2}{(s-M_Z^2)^2 + s\Gamma_Z^2} \quad . \tag{4}$$

This form illustrates the experimentally accessible parameters, M_Z, Γ_Z, and σ_Z, and the relativistic Breit–Wigner used to characterize the resonance. The peak cross section, σ_Z, is related to the standard model coupling strengths by

$$\sigma_Z = \frac{G_F^2 M_Z^4}{6\pi\Gamma_Z^2}(v_e^2+a_e^2)(v_f^2+a_f^2) \quad . \tag{5}$$

In practice, the lowest order line shape defined by Eq. (4) is distorted by radiative effects. The set of diagrams contributing to the first order corrections are shown in Fig. 2. The diagrams 2a and 2b represent the radiation emitted by

the initial state electron. Since this initial state radiation carries energy away, leaving the annihilation center-of-mass energy below the nominal value, it is principally responsible for the distortions to the resonance line shape. Vertex corrections to the initial state and vacuum polarization graphs (Figs. 2c and 2d) represent the electron form factor and charge screening terms, respectively. As they do not change the kinematics, they enter as overall factors to change the scale of the cross section. The vacuum polarization diagrams may be easily summed to all orders in the leading log approximation, but the vertex corrections are complicated and have been only recently calculated to second order.[3,4] Final state radiation and vertex corrections (Figs. 2e–2g) differ from the corresponding initial state diagrams in that they do not alter the center-of-mass energy, and may be summed over inclusively. This summing cancels large logarithmic effects like those associated with the initial state,[5] leaving a correction of $1 + 3\alpha Q^2/4\pi$. The last set of graphs in Fig. 2 are box diagrams, Figs. 2h–2i. These diagrams, if they contain photons only, are known to be odd in $\cos\theta$, so that they contribute to the forward-backward asymmetry, A_{FB}, but make no change to the total cross section. The $\gamma - Z$ pieces have almost the same effect, but in addition contribute a small correction to the cross section. Finally, there are the processes involving interference between initial state photon emission (Figs. 2a and 2b) and final state photon emission (Figs. 2e and 2f). We will omit the box and interference terms in the rest of this paper. We note that a vacuum polarization diagram for the Z^0 is not included because we are using the physical Z^0 mass in the Breit–Wigner.

There are other first order radiative corrections which, *a priori,* must be considered. Corrections coming from one-loop electroweak effects are of order[6] $\alpha/2\pi \sim 0.1\%$. Since these modify the coupling strengths, but have no effect on the kinematics, only the cross section is altered, and that at a level to which experiments will be insensitive. Electroweak radiative corrections might be observable in the comparison of high precision measurements of the Z^0 mass with polarized electron asymmetries where nonstandard model physics can cause deviations in

the measured left-right asymmetry. These would show up as a discrepancy in the weak couplings derived from the measurement of the resonance position, and the weak couplings derived from the asymmetry measurements. QCD corrections arising from final state gluon radiation introduce corrections of α_s/π, where uncertainty in the value of α_s leaves a residual uncertainty of about 1%. This 1%, however, is on the normalization. It is clear that for the mass and width measurement, and measurements of the total cross section, our greatest concerns are the QED corrections coming from initial state radiation.

Since bremsstrahlung from the initial state electrons means that the actual center-of-mass energy available for the annihilation is reduced from the nominal $\sqrt{s} = 2E$ set by the beam energies, one is sampling all energies below $\sqrt{s}$ according to a sampling function determined by the physics of bremsstrahlung. For photons of energy k, the actual center-of-mass is $\sqrt{s(1-k/E)}$ and the observed cross section is given by a convolution,

$$\sigma_{obs}(s) = \int f(k/E, s)\sigma_0(s(1-k/E))dk \tag{6}$$

where the function $f(k/E, s)$ must be computed from the QED diagrams. With $f(k/E, s)$ in hand, one may use Eq. (6) to extract the three parameters of the underlying Breit–Wigner.

The amplitude for the annihilation with one accompanying bremstrahlung photon in the initial state, as in Figs. 2a and 2b, is related to the amplitude for the lowest order process, A_0, by a kinematic factor:

$$A_1 = e\left(\frac{p^+ \cdot \epsilon}{k \cdot p^+} - \frac{p^- \cdot \epsilon}{k \cdot p^-}\right) A_0 \quad . \tag{7}$$

The momenta p^-, p^+, and k refer to the electron, positron, and photon, respectively. Summing over photon polarizations (ϵ) and integrating over photon angular variables, one finds the change in the cross section due to initial state radiation is:

$$d\sigma \sim \sigma_0(s)\left[\frac{2\alpha}{\pi}\left(\log\frac{s}{m_e^2}-1\right)\frac{dk}{k}\right] \quad , \tag{8}$$

where we have assumed the emitted photon energy, k, is small compared to the beam energy in going from Eq. (7) to Eq. (8). It is customary to define an effective coupling constant for bremsstrahlung: $\beta \equiv \frac{2\alpha}{\pi}\left(\log\frac{s}{m_e^2}-1\right)$. This factor is associated with every bremsstrahlung vertex and is large ($\beta = .109$ at SLC energies) due to the large phase space for an electron to split into an electron and a nearly collinear photon. A large effective coupling constant is the first of two major reasons that QED corrections are so large at the Z^0.

Integrating Eq. (8) over a range of bremsstrahlung energies from k_{min} to k_{max} and adding in the zeroth order cross section, one finds the total cross section including single photon emission from the initial state is:

$$\sigma_1(s) = \sigma_0(s)(1+\beta\log\frac{k_{max}}{k_{min}}) \quad . \tag{9}$$

The infrared divergence as $k_{min} \to 0$ is removed with the inclusion of the vertex correction Fig. 2c, leaving

$$\sigma_1(s) = \sigma_0(s)(1+\delta_1+\beta\log\frac{k_{max}}{E}) \quad , \tag{10}$$

where $\delta_1 = \frac{3}{4}\beta + \frac{2\alpha}{\pi}\left(\frac{\pi^2}{6}-\frac{1}{4}\right)$ is sometimes called the first order electron form factor. In order to evaluate Eq. (10), we need to know what k_{max} is. In general, photon energies may extend up to the kinematic limit, just shy of the beam energy E, but a resonant cross section will cut off contributions from hard photons. This means that in the vicinity of the peak, ($2E = M$), the resonance imposes an effective upper limit at $k_{max} \sim \Gamma/2$, so that

$$\sigma_1(s) \sim \sigma_0(s)\,(1+\delta_1+\beta\log\Gamma/M) \quad . \tag{11}$$

The correction δ_1 arises from the effect of the virtual photon cloud, and has a magnitude at the Z^0 of $\delta_1 = +8.7\%$, while the logarithmic term $\beta\log\Gamma/M$ is

due to real radiation,[7] and has a magnitude at the Z^0 of about $\beta \log \Gamma/M \approx -38\%$. In the absence of a resonance, there would be no natural cut-off to k_{max}, and the correction term $\beta \log \Gamma/M$ would disappear. In general, the size of the correction depends on the fractional width of the resonance, Γ/M. This correction is particularly large for a narrow resonance, such as the J/ψ, and is still quite significant at the Z^0 where $\Gamma/M \sim 3\%$. Hence the second reason why the QED corrections are large: the narrow resonance simply cuts off contributions from all but the softest radiative events which, in turn, constitute only a fraction of the total cross section. More physically, the harder radiation simply moves the center-of-mass energy off the resonance into a region of low cross section.

Eq. (10) may be rewritten as

$$\sigma_1(s) = \sigma_0(s)(1+\delta_1)(1+\beta \log \frac{k_{max}}{E}) \quad , \tag{12}$$

provided we agree to drop terms that are higher than first order. This form of the cross section will become more useful as we progress to higher order versions. For the time being we note simply that Eq. (12) separates the virtual corrections $(1+\delta_1)$ from the real $(1+\beta \log \frac{k_{max}}{E})$.

To this point, we have only considered changes to the cross section due to soft photon ($k \leq k_{max} << E$) emission. In this region one may safely ignore the variations of the cross section, and σ_0 can be treated as a constant in Eq. (10). The contributions from photons radiated with $k_{max} < k < E$ must be included, however, and the variation of the cross section with $\sqrt{s}$ taken into account. The bulk of this so-called hard photon contribution could be handled by writing $\sigma_0 = \sigma_0(s')$ where $s' = s(1-k/E)$ is the center-of-mass energy remaining for the annihilation after the photon is radiated, and by allowing $k_{max} \rightarrow E$ in the integration of Eq. (8). There are, however, bremsstrahlung terms which go not as k^{-1}, but as k^0 and k^1. These terms were lost in the approximation between Eqs. (7) and (8), and must be reinstated. The full differential cross section is

$$\frac{d\sigma_1(s)}{d\kappa} = \beta(\frac{1}{\kappa} - 1 + \frac{\kappa}{2})\sigma_0(s') \quad , \tag{13}$$

where now κ is the scaled photon energy previously denoted k/E. Denoting k_{max}/E by κ_0, we write the complete cross section to first order as follows:

$$\sigma_1(s) = \sigma_0(s)(1 + \delta_1 + \beta \log \kappa_0) + \int_{\kappa_0}^{1} \frac{d\sigma_1}{d\kappa} d\kappa \quad , \tag{14}$$

with $d\sigma_1/d\kappa$ being given by Eq. (13). The division of the cross section in Eq. (14) is driven by the need to combine bremsstrahlung and vertex diagrams analytically as $\kappa \to 0$, but leads to the unfortunate presence of an unphysical parameter, κ_0. For analytic calculations, the value chosen for κ_0 is of no consequence, but in Monte Carlo work, where the "soft" cross section [the first term of Eq. (14)] and the "hard" cross section [the second term in Eq. (14)] may be treated separately, difficulties can arise. The desire to set κ_0 as low as possible is hampered by the fact that the first order soft cross section becomes negative. At the same time, values of κ_0 comparable to, or larger than, Γ_Z are prohibited.[8] These problems all evaporate when higher orders are included.

2. Higher Order QED Corrections

Several recent publications have extended calculations of the QED radiative corrections to the Z^0 resonance to second order.[3] [9-11] For $\kappa_0 << 1$ Ref. 9 gives

$$\sigma_2(s) = \sigma_0(s)(1 + \delta_1 + \delta_2 + \beta \log \kappa_0 + \delta_1 \beta \log \kappa_0 + \frac{1}{2}\beta^2 \log^2 \kappa_0) \quad , \tag{15}$$

where the photon energy variable, κ_0, is understood to refer to the *total* radiated energy due to both photons. The second order virtual correction δ_2 is given by[12]

$$\begin{aligned} \delta_2 = \left(\frac{\alpha}{\pi}\right)^2 \Bigg\{ & \left[\frac{9}{8} - 2\zeta(2)\right] \log^2 \frac{s}{m_e^2} \\ & + \left[-\frac{45}{16} + \frac{11}{2}\zeta(2) + 3\zeta(3)\right] \log \frac{s}{m_e^2} \\ & - \frac{6}{5}[\zeta(2)]^2 - \frac{9}{2}\zeta(3) - 6\zeta(2)\log 2 + \frac{3}{8}\zeta(2) + \frac{57}{12} \Bigg\} \end{aligned} \tag{16}$$

where $\zeta(2) = \frac{\pi^2}{6}$, and $\zeta(3) = 1.202$.

As was done for the first order case, this result may be written in product form, again assuming one drops the cross terms that exceed second order:

$$\sigma_2(s) = \sigma_0(s)(1+\delta_1+\delta_2)(1+\beta\log\kappa_0+\frac{1}{2}\beta^2\log^2\kappa_0) \quad . \tag{17}$$

The terms take the following values on resonance, (using $\kappa_0 = \Gamma/M$): $\delta_1 = +8.7\%$, $\delta_2 = -0.5\%$, $\beta\log\kappa_0 = -38\%$, and $\frac{1}{2}\beta^2\log^2\kappa_0 = +7.5\%$. The virtual corrections (δ_1, δ_2,...) are falling rapidly, and already the second order virtual correction, at -0.5%, is below the level of our experimental sensitivity. This is fortunate, because these terms can be gotten only through direct calculation, a daunting task in third order. The real corrections, on the other hand, are larger and falling more slowly, so one reasonably expects the next order to be significant. For these terms, however, a technique exists to deal with all orders.

Before proceeding to higher orders, we note first that, as with the first order calculation, it is necessary to include the contribution from cases where the total radiated energy, κ, lies in the range $\kappa_0 < \kappa < 1$. To second order, the differential cross section analogous to the first order result in Eq. (13) is given in Ref. 9:

$$\begin{aligned}\frac{d\sigma_2(s)}{d\kappa} = \sigma_0(s')\Bigg[&\beta\left(\frac{1}{\kappa}-1+\frac{\kappa}{2}\right)(1+\delta_1+\beta\log\kappa) \\ &+(\frac{\alpha}{\pi})^2\left(\frac{1+(1-\kappa)^2}{\kappa}A(\kappa)+(2-\kappa)B(\kappa)+(1-\kappa)C(\kappa)\right)\Bigg] \quad ,\end{aligned} \tag{18}$$

where $s' = s(1-\kappa)$, and the functions $A(\kappa)$, $B(\kappa)$, and $C(\kappa)$ are included for convenience in the Appendix. The purely second order $(\frac{\alpha}{\pi})^2$ pieces augment the total cross section slightly at values of $\sqrt{s} > M_Z$, but their impact is small. At values of $\sqrt{s}$ up to 5 GeV above the resonance, the net effect is less than 0.4%. Exactly as was done in first order, Eq. (14), one may write the total cross section to second order as the sum of the soft part, Eq. (15), and the integral over the hard part, Eq. (18).

The real corrections may now be treated to all orders. The separation of virtual and real corrections achieved by the factorized forms of the cross section, Eqs. (12) and (17), is useful here. By comparing these equations, one sees that the real correction contributed at n^{th} order takes the general form

$$(\frac{\alpha}{\pi})^n(\log\frac{s}{m_e^2}-1)^n(\log\kappa_0)^n \quad . \tag{19}$$

Such terms include the well-known leading logs which dominate the contribution from each order. Nonleading terms of the form

$$(\frac{\alpha}{\pi})^n(\log\frac{s}{m_e^2}-1)^m \tag{20}$$

with $m < n$ appear in the virtual correction, and other nonleading terms show up in the cross terms that arise in the product of real and virtual corrections. The fact that the leading logs may be summed to all orders[13] allows one to extend Eq. (17) with the formalism known as exponentiation:

$$\begin{aligned}\sigma(s) &= \sigma_0(s)(1+\delta_1+\delta_2) \\ &\qquad \left(1+\beta\log\kappa_0+\frac{1}{2!}\beta^2\log^2\kappa_0+\frac{1}{3!}\beta^3\log^3\kappa_0+\ldots\right) \\ &= \sigma_0(s)(1+\delta_1+\delta_2)\exp(\beta\log\kappa_0) \\ &= \sigma_0(s)(1+\delta_1+\delta_2)(\kappa_0)^\beta \quad .\end{aligned} \tag{21}$$

For the extraction of the Z^0 line shape, this is a particularly powerful result, because it takes precisely those terms responsible for the line shape distortions, and sums them to all orders. This bodes well for the extraction of M_Z and Γ_Z. Virtual corrections are computed only to second order, but they affect mostly the overall normalization, and at a level already below experimental systematic errors. It is worth noting that through the product with δ_1 and δ_2, the next-to-leading and next-to-next-to-leading terms are also included.

For a complete treatment, exponentiation must also be included in the hard part of the cross section, the part given in first order by Eq. (13), and in second order by Eq. (18). The correct prescription for doing so may be inferred by comparing the derivative of Eq. (21), $d\sigma_{exp}/d\kappa$, with the $\kappa \to 0$ limit of Eq. (18) or Eq. (13). From Eq. (21) one obtains

$$\frac{d\sigma_{exp}}{d\kappa} = \beta \frac{1}{\kappa} \sigma_0(s) \left[(1 + \delta_1 + \delta_2) \kappa^\beta \right] \quad . \tag{22}$$

Expanding the quantity in brackets as a series in β, and retaining only terms up to β^2, one finds

$$\frac{d\sigma_{exp}}{d\kappa} = \beta \frac{1}{\kappa} \sigma_0(s) (1 + \delta_1 + \beta \log \kappa) \quad . \tag{23}$$

This form correctly reproduces the $\kappa \to 0$ limit of the second order hard cross section, Eq. (18), and one sees easily that the same limit of the first order hard cross section, Eq. (13), is reproduced if only terms up to β^1 are retained in Eq. (23). One concludes therefore that exponentiation is properly included in the first order and second order hard cross sections by writing

$$\frac{d\sigma_{1exp}}{d\kappa} = \sigma_0(s') \beta (\kappa^{\beta-1}(1 + \delta_1) - 1 + \frac{\kappa}{2}) \tag{24}$$

and

$$\begin{aligned} \frac{d\sigma_{2exp}}{d\kappa} = \sigma_0(s') \Bigg[& \beta \left(\kappa^{\beta-1}(1 + \delta_1 + \delta_2) - 1 + \frac{\kappa}{2} \right) \\ & + (\frac{\alpha}{\pi})^2 \left(\frac{1 + (1-\kappa)^2}{\kappa} A(\kappa) + (2 - \kappa) B(\kappa) + (1 - \kappa) C(\kappa) \right) \Bigg] . \end{aligned} \tag{25}$$

We note that with the leading log summation of infrared photons, the familiar κ^{-1} spectrum of single bremsstrahlung has become $\kappa^{\beta-1}(1 + \delta_1 + \ldots)$. The presence of the β in the exponent indicates a softer spectrum than expected from single photon bremsstrahlung, and this softening will be seen later to have a significant impact on the Z^0 line shape.

For a complete result with all corrections to second order, and leading logs summed to all orders, we have

$$\sigma_{obs}(s) = \sigma_0(s)(1+\delta_1+\delta_2)\,\kappa_0^{\beta} \; + \int_{\kappa_0}^{1} \frac{d\sigma}{d\kappa}\,d\kappa \quad , \tag{26}$$

with $d\sigma/d\kappa$ taken from Eq. (25). The κ_0 problem that arose in the first order calculation is no longer present in Eq. (26) because the soft term vanishes in a well-behaved fashion as $\kappa_0 \to 0$. This allows one to set κ_0 arbitrarily small. In fact, under the (good) approximation that $A(\kappa) = B(\kappa) = C(\kappa) = 0$, one may set κ_0 to zero and the integral can be solved analytically. This has been done by Cahn,[14] with the additional but not necessary approximation that $\delta_2 = 0$. The result is an analytic expression for $\sigma_{obs}(s)$ that is suitable for fitting acceptance-corrected data. For the reader's convenience, it is reproduced in the Appendix.

At this point it is instructive to review what has been accomplished by the inclusion of higher order corrections, and ask whether the primary goal of bettering the experimental systematic errors on M_Z, Γ_Z, and σ_Z has been achieved. Following Ref. 9, we illustrate in Fig. 3 the expected line shape for $\mu-$pair final states, $\sigma_{obs}^{\mu\mu}(s)$, under four levels of radiative correction: (1) pure first order, (2) first order with exponentiation, (3) pure second order, and (4) second order with exponentiation. For clarity, the full expressions for $\sigma_{obs}(s)$ are given in the Appendix. The underlying Breit–Wigner in these calculations has $M_Z = 93.0$ GeV/c^2, $\Gamma_Z = 2.5$ GeV, and $\sigma_Z = 1.86$ nb.

The peak of the first order calculation is shifted to 93.180 GeV/c^2, and peak cross section lowered to 1.313 nb, a 29% drop relative to the cross section of the underlying resonance. These numbers are consistent with expectations. When exponentiation is included with the first order calculation, the peak position moves back to 93.108 GeV/c^2, and the peak height to 1.382 nb. The line shape with exponentiation more closely resembles the underlying shape because exponentiation weights the soft radiation more heavily than the pure first order calculation. The first order calculation properly represents hard radiation, but

badly underrepresents the soft components. In first order, for instance, approximately 50% of the cross section occurs below $\kappa_0 = 0.01$, while the inclusion of exponentiation changes this to 90%. Thus the first order correction shifts the peak position too much to the high side and smears the narrow profile into a lower, broader one.

It is interesting to compare second order with exponentiation to first order with exponentiation. Figure 3 shows there is *no* difference in the peak position, which also occurs at 93.108, but there is a drop in the peak height from 1.382 to 1.372 nb. This latter effect can be traced almost entirely to the inclusion of the second order virtual correction δ_2. The important conclusion here is that *the leading logs dominate all line shape distortions.* The explicit presence of nonleading terms to second order has little effect on the position of the peak.

Finally a comparison of the pure second order with the exponentiated second order rounds out the picture. The second order line shape shows a peak at 93.092, with a peak height of 1.374 nb. This peak position is lower than the 93.108 found for the exponentiated case, indicating that the second order real term has overcompensated the excesses of first order. The peak height is almost identical with that of exponentiated second order, as one would expect since they share identical nonleading terms.

Little can be said about the effect of the various correction schemes on the width, Γ_Z, without a more quantitative approach. To meet this need, a set of "fake data" was generated using an exponentiated second order version of $\sigma_{obs}(s)$ (see the Appendix) to represent the "true" resonance shape. The relative accuracy of a particular correction scheme can then be determined by fitting this "data". The fitting procedure consists of the minimization of a χ^2 function with respect to the underlying resonance parameters M_Z, Γ_Z, and σ_Z of Eq. (4). Table 1 summarizes the results, given in terms of the differences between the values of the parameters found in the fit and those used to generate the "data". The results were found not to depend in any significant way on the choice of scan

strategy, *i.e.*, the particular set of center-of-mass energies and their statistical weights. Nor do they depend on details of the χ^2 minimization procedure. The results therefore represent a reasonable comparison of the intrinsic accuracy of the correction schemes. This procedure is used here (Table 1) to compare general levels of approximation relative to the most complete level presently available (Ref. 9). It is also invoked later to compare the results of various authors.

Table 1 indicates that a first order calculation is clearly inadequate, as it misses the true mass by 121 MeV/c^2, almost three times the expected experimental systematic error, and misses the width by 152 MeV, which is equivalent to almost one light neutrino generation (176 MeV). By contrast, both the exponentiated first order and pure second order perform acceptably well, the former being somewhat better, but both being within the limits of experimental systematics.

From these observations we draw the following conclusions. First, the virtual corrections affect mostly normalization, so accounting for them to second order is quite adequate given the known systematic errors on luminosity measurements. Second, the real terms account for the distortion of the line shape, and must be summed to all orders. Once this summation is done, the mass and width can be properly extracted with an accuracy of a few MeV. Third, the nonleading terms at second order have been shown explicitly to play no significant role in the extraction of mass and width.

To this point we have dealt only with the corrections arising from initial state radiative effects, on the justifiable grounds that the other contributions, from final state radiation, box diagrams, and so forth are small even in first order. The ability to factorize the initial state effects from the remainder of the cross section is a powerful tool. One may carry this notion further to assign these radiative effects to a *structure* of the initial state. In this view, the sampling function, $f(k/E,s)$ in Eq. (6), arises from the product of electron structure functions,

$$\int dk_1 D_e(k_1,s) D_e(\frac{k-k_1}{1-k_1/E},s) = f(k/E,s) \quad , \tag{27}$$

which describe the probability to find the electron having radiated off an amount of energy k_1 or $k - k_1$. Without changing the results, this alteration of one's point of view introduces a very useful technique long familiar in hadron physics, but only recently applied to e^+e^- physics.

3. The Structure Function Approach

An electron radiating a photon of energy k is left with a fraction $x = 1 - k/E$ of its original energy. This electron may go on to participate in the annihilation, $e^+e^- \to Z^0, \gamma$, or may split off more photons. The photons themselves may split into e^+e^- pairs, members of which may participate in the annihilation. Either way, the electron finally annihilating carries only some fraction x of the nominal beam energy E. The cascading of electrons and photons is illustrated in Fig. 4. In the standard notation, the probability distribution for finding an electron of momentum fraction x in an interaction with center-of-mass energy $\sqrt{s}$ is written $D_e(x,s)$. For an electron and positron of momentum fractions x_1 and x_2, respectively, the total center-of-mass energy is $\sqrt{x_1 x_2 s}$, and the cross section is $D_e(x_1,s)\sigma_0(x_1x_2s)D_e(x_2,s)$. The total observed cross section is then

$$\sigma_{obs}(s) = \int_\mu^1 dx_1 \int_\mu^1 dx_2 D_e(x_1,s)\sigma_0(x_1x_2s)D_e(x_2,s) \quad ; \tag{28}$$

the lower integration limit depends on the mass of the final state particles. The $D(x,s)$ satisfy the normalization and momentum conservation equations:

$$\begin{aligned} \int D_e(x,s)dx &= 1 \quad , \\ \sum_i \int x D_i(x,s)dx &= 1 \quad . \end{aligned} \tag{29}$$

The first integral includes all electron components (*i.e.*, valence and sea electrons), while the sum in the second formula runs over all the available partons,

photons included. It is safe to neglect all other components, because real heavy fermion pairs are strongly suppressed, and one more pair of electrons can be produced only in fourth order.

The concept of the structure function has been borrowed from QCD where its application in the description of hadrons has proven fruitful. Evolution equations were written for a vectorial theory in the early 1970s[15–18] and were first applied to QCD in Ref. 18. More recently, they have been used to calculate QED radiative corrections in Ref. 3; subsequently, other calculations have been done[10][11] for specific application to the Z^0 energy region. By including a complete second order evolution of the initial state, including the graphs of Fig. 5, the structure function is

$$D_e(x,s) = D_{e\gamma}(x,s) + D_{eee}(x,s) \quad . \tag{30}$$

$D_{e\gamma}(x,s)$ refers to the probability of finding an electron of momentum fraction x plus an arbitrary number of photons, while $D_{eee}(x,s)$ refers to the probability of finding an electron of momentum fraction x, plus an electron-positron pair, plus an arbitrary number of photons. Reference 3 yields the following result for $D_{e\gamma}(x,s)$ and $D_{eee}(x,s)$:

$$\begin{aligned} D_{e\gamma}(x,s) &= \frac{\beta}{2}(1-x)^{\frac{\beta}{2}-1}\Big(1+\frac{3}{8}\beta-\frac{\beta^2}{48}\big(\frac{1}{3}L+\pi^2-\frac{47}{8}\big)\Big)-\frac{1}{4}\beta(1+x) \\ &\quad+\frac{1}{32}\beta^2\Big(4(1+x)\log\frac{1}{1-x}-\frac{1+3x^2}{1-x}\log x-5-x\Big)\ , \end{aligned} \tag{31}$$

$$\begin{aligned} D_{eee}(x,s) &= \theta(1-x-\frac{2m_e}{E})(\frac{\alpha}{\pi})^2\Big[\frac{1}{12}\frac{(1-x-2m_e/E)^{\beta/2}}{1-x}(L_1-\frac{5}{3})^2 \\ &\quad\Big(1+x^2+\frac{1}{6}\beta(L_1-\frac{5}{3})\Big)+\frac{1}{4}L^2\big(\frac{2}{3}\frac{(1-x^3)}{x}+\frac{1-x}{2}+(1+x)\log x\big)\Big]\ , \end{aligned}$$

where $L=\log(s/m_e^2)$, β has been defined above, $L_1 = L+2\log(1-x)$ and θ is the Heavyside function. Substituted into Eq. (28), one may derive the form of $f(k/E,s)$ in Eq. (6), as given in the Appendix.

These calculations of $D_e(x,s)$ in QED assume *collinear* radiation, so the (small) effect of photons emitted at large angles is not included. The collinear and nearly-collinear radiation dominate the center-of-mass energy shifts and the $\mu-$pair acollinearities, but the $\mu-$pair aplanarity is determined by photons of large transverse momentum. For a full treatment of the kinematics, this transverse momentum must be accounted for. This can be done in two different ways:

1. The first is to assume the photon p_T distribution is properly simulated by first order calculations. Since the only photons that will have significant kinematic impact are those with large p_T, this is a very good approximation. One may then include the matrix element for hard photon emission[10] in the σ_0 of Eq. (28).

2. The second is to compute directly the structure function $D_e(x,p_T,s)$ as has been done in the QCD case.[20]

In either case, the nonfactorizable pieces, such as box and interference terms, may be added by hand. These will then modify the σ_0 of Eq. (28).

The removal of energy by bremsstrahlung photons changes not only the center-of-mass energy, $\sqrt{s}$, but also the center-of-mass momentum. In general, the annihilation center-of-mass is no longer at rest with respect to the reference frame of the detector. For $\mu-$pair final states, the resulting acollinearities and aplanarities are detectable kinematic effects which provide the only experimental check one has on the radiative correction calculations. Since collinear radiation of energy κE results in a $\mu-$pair acollinearity $\varsigma \approx \kappa$, an acollinearity resolution of 10 mr allows one to check the corrections directly for $0.01 < \kappa < 1$. The bulk of the corrections arise from infrared radiation, $\kappa \leq 0.01$, but the normalization constraints such as those of Eq. (29) impose a relationship between the hard and soft pieces so that the kinematic effects may remain useful checks on the entire calculation. A bremsstrahlung photon of transverse momentum $\kappa_T E$ results in an aplanarity $\eta \approx \kappa_T$, and thus offers a similar check on the transverse elements of the calculation.

One may hope to exploit these kinematic manifestations to measure the structure function $D_e(x,s)$. If such a measurement is performed on PEP/PETRA data, the resulting structure functions may be evolved to SLC energies and used as input to an SLC Monte Carlo. Amplifying on these ideas, one notes that the center-of-mass energy is given by $\sqrt{x_1 x_2 s}$, and additionally, the Lorentz boost, β, of the center-of-mass is given by $\beta = (x_1 - x_2)/(x_1 + x_2)$. With the Lorentz dilatation given by $\gamma = (x_1 + x_2)/2\sqrt{x_1 x_2}$, one can directly write down the acollinearity of a $\mu-$pair final state arising from the annihilation of an electron and positron of momentum fractions x_1 and x_2, respectively, as

$$\varsigma = \left| \frac{2\beta\gamma \sin\theta'}{1 + \beta^2\gamma^2 \sin^2\theta'} \right| \quad , \tag{32}$$

where θ' is the emission angle of the μ^+ in the $\mu-$pair rest frame. The moments of the acollinearity distribution of a $\mu-$pair sample will then be given by

$$f^n(\varsigma, s) = \int dx_1 dx_2 d\theta' \frac{1}{\sigma} \frac{d\sigma_0}{d\theta'} D_e(x_1, s) D_e(x_2, s) \varsigma^n \quad . \tag{33}$$

In the PEP/PETRA region, and in other energy regions where a good amount of data on the continuum has been collected, the underlying Born cross section is known much better than 1%, and with a suitable Monte Carlo, the acollinearity distribution for μ pairs gives a direct measurement of the electron structure function, using Eq. (33). In the same way, the measurement of the p_T dependence of the structure functions can be measured from aplanarity distributions, where the aplanarity η is defined as

$$\eta = \frac{|\vec{p}_{T+} \times \vec{p}_{T-}|}{|\vec{p}_{T+}| \cdot |\vec{p_{T-}}|} \quad . \tag{34}$$

In the SPEAR region, the abundance of resonant states and the large α_s imply that there are nonperturbative and theoretically unpredictable QCD effects affecting the total hadronic cross section. Most of the results published used

Ref. 21 to extract the QED effects, where the lack of proper form factors can affect the normalization at the 10% level, and missing hard pieces have the side effect of changing the total cross section when hard radiation can take s' down to the region of a large resonance. Besides the interest of reviewing old data using new calculations, there is a small change on the correction Δr[22] to $\alpha(M_Z^2)$ obtained with a dispersion relation fit of the low energy data.

4. Comparison of Existing Calculations

We have cited several works (Refs. 3, 9, 10, 11 and 14) in which QED corrections beyond first order have been calculated. Broad differences of approach (matrix element, structure function) have been noted, but differences of detail and discrepancies in results have been reserved for this section. Since the treatment of real pairs differs among authors,[12] we have adopted the following convention for the sake of consistency in these comparisons: real pairs are ignored in Ref. 3, and the electron form factor of Ref. 11 was set equal to the δ_2 of Ref. 9. Hence these results all include virtual pairs, but not real pairs. We have not attempted here to include all existing calculations. In particular, evaluation of the results displayed in Refs. 10 and 23 are expected to be numerically similar to the aforementioned papers. To complete the review and establish a familiar reference point, we include the classic work of Jackson and Scharre, Ref. 21, where we have modified the virtual correction to exclude the (small) photon vacuum polarization, which is not relevant at the Z^0.

Two types of comparison are made. The first is done by choosing three parameters, $M_Z = 93.0$ GeV/c^2, $\Gamma_Z = 2.5$ GeV, and $\sin^2\theta_W = 0.230$ and generating the profile σ_{obs} according to the corrections given in each of these references. For the $\mu^+\mu^-$ final states, Table 2 gives the cross sections at several values of $\sqrt{s}$ in terms of a deviation in percent from the prediction of Ref. 9. The very close agreement between Ref. 9 and Refs. 11 and 3 is quite striking in view of the fact that the former is strict matrix element calculation plus exponentiation, and the

latter are structure function results. The large disagreement between Ref. 9 and Ref. 21 may be attributed to incomplete treatment of virtual terms, as discussed below.

The "fake data" test used earlier to compare levels of radiative correction may be applied here to compare the agreement on M_Z, Γ_Z, and σ_Z that use of various authors' works would yield. Table 3 shows the results. Again we see the close agreement between Refs. 9, 3 and 11. The shape of the resonance is also well described by Ref. 14. This result has the advantage of a compact, analytic formulation. We have used the sum of the "hard" and "soft" photon results from Ref. 14 for this comparison.

We see that the result of Ref. 21 has substantial discrepancy compared to the more recent calculations, for which the overriding cause is as follows. The corrected cross section with exponentiation of soft photons to all orders, and with virtual and hard photon corrections to first order can be taken from Eqs. (25) and (26)[dropping the δ_2 and $(\alpha/\pi)^2$ terms, and letting $\kappa_0 \to 0$]:

$$\sigma_{obs}(s) = \beta \int \sigma_0(s')\,\kappa^{\beta-1}(1+\delta_1)\,d\kappa \;-\; \beta \int \sigma_0(s')\,(1-\frac{\kappa}{2})\,d\kappa \quad , \tag{35}$$

where $s' = s(1-k/E) = s(1-\kappa)$, as before. The second term (hard photon bremsstrahlung), is ignored for the remainder of this discussion. This convolution then takes on the general form

$$\sigma_{obs}(s) = \int \sigma_0(s')\,f(\kappa,s)\,(1+\delta_1)\,d\kappa \quad . \tag{36}$$

In Ref. 21, however, the integral is broken up into two terms

$$\sigma_{obs}(s) = \int \sigma_0(s')\,f(\kappa,s)\,d\kappa \;+\; \delta_1\,\sigma_0(s) \quad . \tag{37}$$

In this case, the virtual correction δ_1 modifies the cross section only at the energy $\sqrt{s}$. The reason that this approximation breaks down is illustrated by considering

a situation where the center-of-mass energy is slightly above a narrow resonance of mass M_R, so that $\sqrt{s} = M_R + \Delta E$. The virtual correction shown in Fig. 6 has a small effect which is correctly included in the δ_1 term in both Eq. (36) and Eq. (37). The emission of bremsstrahlung radiation of energy near ΔE represents, on the other hand, a very large effect, and the process depicted in Fig. 7 of a virtual correction along with emission of photons down to the resonance peak is relatively important. Such contributions are not included in Eq. (37). The numerical significance of this omission can be seen in Tables 2 and 3 by comparing Ref. 21 to Ref. 14, wherein the most significant difference is the distinction between Eq. (36) and (37). Because Ref. 21 has been used extensively to extract physics results, this distinction is potentially important. It is discussed further in the last section.

Previous discussion indicated that several calculations possess sufficient accuracy for the extraction of the parameters of the Z^0 resonance. We now see that there is excellent agreement between the most complete of these results, *i.e.,* Refs. 3, 9 and 11. The simplified result of Ref. 14 is, in fact, also sufficiently accurate, given the expected experimental errors. Although the authors represented in Tables 2 and 3 include different levels of approximation for the virtual and hard photon contributions to the cross section, they all include some form of exponentiation of the soft photons. This is not too surprising, as Table 1shows that an excellent approximation is achieved by including exponentiation of soft photons along with other corrections to only first order.

5. Monte Carlos

In the course of this work, two Monte Carlo programs have been developed. The first is based on the MMG1 program[19] which embodies the complete first order calculation, and has been widely used in analysis of PEP and PETRA data. MMG1 has been modified to include the second order and exponentiation corrections, as in Eq. (26), and shall be referred to here as MMGE. The second program is based on the structure function analysis of Ref. 11. We give a brief review of each program here.

The starting point of MMG1 is the radiation spectrum, $d\sigma/d\kappa$, which is used to generate the photon energy. All other kinematic variables are generated subsequently. The final result is a set of four vectors for the produced fermion pair, and a four vector for the photon if its energy was generated above κ_0. Normally[8] $\kappa_0 = 0.01$. In MMGE, the radiation spectrum is taken from Eq. (26). The energy generated from this spectrum is then assigned to a single photon, and the remainder of the program proceeds in the usual fashion. Final state radiation, box diagrams, initial/final state interference, and photon vacuum polarization corrections are turned off. The use of exponentiation allows κ_0 to be set arbitrarily small, and typically $\kappa_0 = 0.0001$ is used. As an example of this program's application, Fig. 8 shows the effect of higher order corrections on the forward-backward $\mu-$pair asymmetry, calculated with MMGE. One sees that, characteristically, the first order calculation exaggerates the correction, and with higher orders, the final result lies between the lowest order and the first order expectation.

A drawback to a program of MMGE's nature lies in the approximation that all the radiated energy is carried by one photon. In fact it should be spread over infinitely many photons. In practice, if the radiated energy is large, then it certainly is carried predominantly by one photon, while if the radiated energy is small, the kinematic effects are negligible anyway, so it does not matter. In the middle ground where one might have two photons of comparable energy,

the approximation is poorest, and one may expect to see discrepancies between acollinearity data and predictions of this Monte Carlo.

Equation (30) provides the starting point for the structure function Monte Carlo. With this method one may generate an initial state that already contains all the important radiative corrections, and add further radiative corrections of lesser impact to first order in the matrix element for the hard annihilation process. The kinematics of the final state are largely accounted for by the initial state radiation.

In the structure function Monte Carlo, the momentum fractions x_1 and x_2 are generated first. The center-of-mass frame is then defined, and the fermion four vectors are generated back-to-back in that frame, and boosted to the lab frame. No photon variables are generated; effectively, all radiation is assumed collinear with the beam axis. The fact that collinear radiation accounts for the bulk of the kinematic effects ($\mu-$pair acollinearities, chiefly) make this a useful program. The absence of photon variables may hinder it in some applications. As with MMGE, final state radiation, boxes, and so forth are not presently included.

In both Monte Carlos the κ_0 problems that plague first order programs are eliminated by the exponentiation of infrared photons. The value of κ_0 may be pushed arbitrarily low. The structure function approach has the additional strength that the radiative corrections are explicitly decoupled from the annihilation process. This means that one may use the same program for different processes, simply by substituting the σ_0 of one's choice into Eq. (28). By the same token, beam energy spreads of arbitrary shape are easily included in this program. Both programs give negligible errors on predictions of total cross sections for fermion pairs.

6. Applications

In Sec. 4 we explored the consequences of a separation between soft/virtual terms and radiation terms in the Z^0 energy region. As an interesting application of the current radiative correction calculations, data on the hadronic cross section at the J/ψ resonance[24] were exhumed and refitted.

For this particular case, the beam energy spread $\sigma_E/\sqrt{2}$ is much larger than the natural width of the resonance, and a further integration over all annihilation energies should be considered. Eq. (6) becomes

$$\sigma_{obs}(s_0) = \int dk \int d(\sqrt{s}) f(k/E, s) G(\sqrt{s} - \sqrt{s_0}) \sigma_0((1 - k/E)s) \quad . \tag{38}$$

The energy distribution G is assumed to be gaussian with standard deviation σ_E, and the dependence of f on s can be dropped in this particular case. For the same reason we can change the order of integration and we get

$$\sigma_{obs}(s_0) = \int d(\sqrt{s}) G(\sqrt{s} - \sqrt{s_0}) \int dk f(k/E, s) \sigma_0((1 - k/E)s) \quad . \tag{39}$$

The use of such a formula as a fitting function is still technically almost impossible for this particular case. On one hand, a repeated numerical evaluation of a double integral is prohibitively CPU-time consuming; on the other hand, the available integration algorithms do not easily allow a precise determination ($\lesssim 1\%$) of the integral, because of the almost singular shape of the cross section and of its first derivative respect to s or k.

It is interesting instead to perform the integral over k analytically using the formula given by Cahn[14] and reported in the Appendix, and check the results against the formula given by Ref. 21. In fact, these two recipes are equal but for the different treatment of the virtual terms mentioned in Sec. 4. We checked that the formula by Cahn, integrated over the beam energy spread, was equivalent within $\approx 1\%$ to the results of the structure function Monte Carlo, which is numerically stable. The photon vacuum polarization was taken into account.

For this work we have made first a fit to the resonance using five free parameters: the branching ratio of the J/ψ into electrons B_{ee}, the mass M, the beam energy spread $\sigma_E/\sqrt{2}$, the total width Γ, and the background cross section σ_{bk}. The hadronic cross section at the peak from unitarity considerations is

$$\sigma_{had} = \frac{12\pi}{M^2}\frac{\Gamma_{ee}\Gamma_{had}}{\Gamma_{tot}^2} = \frac{12\pi}{M^2}B_{ee}B_{had} \quad . \tag{40}$$

As a partial constraint to the fit, the sum $(2B_{ee} + B_{had})$ was set equal to one. The minimization program was observed to find three close minima ($\approx 5\%$ apart) along the hyperbola defined by

$$B_{ee}\Gamma = \Gamma_{ee} \sim \text{constant} \sim 4.8\text{keV} \quad . \tag{41}$$

These two parameters, B_{ee} and Γ, could not be constrained separately without using data for e^+e^- and $\mu^+\mu^-$ final states from the same scan. The product, however, is roughly proportional to the area under the resonance peak, a quantity to which this analysis is sensitive. The other three parameters, M, σ_E and σ_{bk}, were tightly constrained. The fit performed with the algorithm of Ref. 21 behaved similarly and gave a partial width into electrons approximately equal to 4.5 keV. These numbers should not be taken as new measurements of the J/ψ leptonic width, because we did not use the leptonic data and there could be differences in the details of this analysis and that of Ref. 24; their interest is only in the comparison between the two results. The present error on Γ_{ee} is .3 keV,[25] and we plan to discuss this discrepancy in a future paper. Finally, the Monte Carlo was run to produce the fit of Fig. 9 with the following parameters: $B_{ee} = .0675$, $M = 3095.02$ MeV, $\sigma_E/\sqrt{2} = .75$ MeV, $\Gamma = 71.0$ keV and $\sigma_{bk} = 21.5$nb, which correspond to the best fit obtained.

In a separate application of the J/ψ data, we may turn around the classic problem of radiative corrections to a resonance, and instead of using radiative corrections calculations to probe the resonance, use the resonance to probe the

radiative corrections. The J/ψ, being much narrower than the combined beam spread and radiative spread of the beam, may be regarded as a delta function. As such, it makes an excellent probe. We take the graph of Fig. 9, subtract the QED background, and replace the abscissa with $2E' = 2(E - E_{nominal})$. What one obtains (Fig. 10) is a mirror image of the resonance that is a precise measurement of a (new) convolution function where beam energy spread effects are taken into account,

$$\begin{aligned} f'(k/E, M^2) = \int & dx_1 d(\Delta E_1)\ \ d(\Delta E_2) \\ & \times D_e(x_1, s)\ \ D_e(\frac{1 - k/E}{x_1}, s) \\ & \times D'(\Delta E_1)\ \ D'(\Delta E_2) \quad , \end{aligned} \tag{42}$$

where $k/E = \kappa = 1 - x_1 x_2$, M is the resonance mass and the convolution of the $D'(\Delta E)$ functions gives the previously defined function $G(\sqrt{s} - \sqrt{s_0})$. We have assumed that $s \simeq M^2$, so that $f(k/E, s)$ does not change during the scan. D' is the beam energy spread (and can include, for example, beamstrahlung as well), and the integration must be performed on ΔE first to take into account the time ordering correctly. Comparing this with Eq. (28) we see that the cross section has dropped out after an integration over $\sqrt{s}$, as the resonance is effectively a Dirac δ-function in this case. Substitution of $f'(k/E, s)$ above into Eq. (6) could then be used as a test of the structure functions, as it is relatively insensitive to small changes of the J/ψ resonance parameters. Measurements of this kind could also be performed at the Υ, which is narrower and sits on a very smooth continuum. These beam energy spread effects, however, are much larger because of the increased critical energy of the synchrotron radiation emitted by the beams.

7. Conclusions

We conclude that while the radiative corrections to the Z^0 resonance are quite large, they can be calculated and incorporated into the comparison with experiment so that there will be no significant theoretical uncertainties on the measurements of the resonance parameters at SLC and LEP. We have shown that the photon bremsstrahlung is a large distortion to the Z^0 resonance because of the large effective coupling constant for a 50 GeV electron to emit a nearly collinear photon, and because the resonance is relatively narrow. We find that we can sum to all orders (exponentiate) just those terms (real photon emission) that are responsible for the line shape distortions, and the virtual corrections, calculated to second order, will mostly affect the overall normalization of the resonance, and that at a level below the expected experimental systematic error. Electroweak radiative corrections need not be included to extract the resonance parameters to sufficient precision.

The ability to factorize the initial state effects from the remainder of the cross section has led to the description of the initial state radiative corrections in terms of structure functions and evolution equations. We discuss this approach and show how the structure function formalism allows us to include effects like beam spread in a natural way.

At least three papers have calculated radiative corrections using independent matrix element and structure function methods. We have directly compared these calculations and several others by using them to fit a resonance shape. The agreements and disagreements between the calculations are understood, and we find that all calculations that include exponentiation of the soft photons and virtual corrections to at least first order are adequate for the measurement of the parameters of the Z^0 resonance. We also find that the analytic fitting function derived by Cahn is suitable for fitting the data. An absolute precision of better than 1% everywhere around the resonance, however, can be achieved only by including (together with soft photons to all orders) form factors and hard pieces

to second order, real pairs to lowest order, and box diagrams and final state corrections to first order. The electroweak corrections do not affect the resonance shape at the 1% level.

We describe Monte Carlos that have been developed in the course of this work. We illustrate the new calculations of radiative corrections by refitting the J/ψ resonance.

It is a pleasure to thank F. Berends, R. Cahn, F. Dydak, B. Lynn and B. Ward for many useful discussions; special thanks to S. Brodsky and L. Trentadue for illuminating the physics content of evolution equations, and to V. Luth for helping exhume the data on the J/ψ.

APPENDIX

In this section we collect those formulae the reader may find useful. These include the functions $A(\kappa)$, $B(\kappa)$, and $C(\kappa)$ from Eq. (18), taken from Ref. 9; the function $\sigma_{obs}(s)$ taken from Ref. 14; the four forms of $\sigma_{obs}(s)$ used to make Fig. 3; and the function $f(k/E,s)$ from Eq. (6) derived from the structure function analysis of Ref. 3.

$A(\kappa)$, $B(\kappa)$, and $C(\kappa)$ are given below:

$$\begin{aligned} A(\kappa) = &- \log^2\frac{s}{m_e^2}\log(1-\kappa) + \log\frac{s}{m_e^2}\left[Li_2(\kappa) - \frac{1}{2}\log^2(1-\kappa)\right. \\ &\left. + \log(1-\kappa)\log(\kappa) + \frac{7}{2}\log(1-\kappa)\right] + \frac{1}{2}\log^2(1-\kappa)\log(\kappa) \\ &+ \frac{1}{2}Li_2(\kappa)\log(1-\kappa) - \frac{1}{6}\log^3(1-\kappa) + \zeta(2)\log(1-\kappa) - \frac{3}{2}Li_2(\kappa) \\ &- \frac{3}{2}\log(1-\kappa)\log(\kappa) - \frac{17}{6}\log(1-\kappa) + \frac{1}{6}\log^2(1-\kappa) \\ &- \frac{1}{\kappa}\log^2(1-\kappa) - \frac{1}{3} - \frac{2}{3\kappa}\log(1-\kappa) - \frac{1}{3\kappa^2}\log^2(1-\kappa) \end{aligned} \tag{43}$$

$$\begin{aligned} B(\kappa) = &\log^2\frac{s}{m_e^2}\left[\frac{1}{2}\log(1-\kappa) - 1\right] \\ &+ \log\frac{s}{m_e^2}\left[\frac{1}{4}\log^2(1-\kappa) - \log(1-\kappa) + \frac{7}{2}\right] \\ &+ \frac{3}{2}Li_3(\kappa) - 2S_{1,2}(\kappa) - \log(\kappa)Li_2(\kappa) - \zeta(2) + \frac{1}{6}\log^2(1-\kappa) \\ &+ \frac{1}{2}\log(1-\kappa)\log(\kappa) - \frac{1}{4}\log^2(\kappa) + \frac{5}{2}\log(1-\kappa) + \frac{3}{2}\log(\kappa) - \frac{1}{6} \end{aligned} \tag{44}$$

$$C(\kappa) = 2\log^2\frac{s}{m_e^2} + \log\frac{s}{m_e^2}\left[\log(1-\kappa) - \frac{13}{2}\right] + \frac{16}{3}\zeta(2)$$
$$- \frac{25}{6}Li_2(\kappa) - \frac{13}{12}\log^2(1-\kappa) - 4\log(1-\kappa)\log(\kappa) \qquad (45)$$
$$+ \frac{3}{2}\log^2(\kappa) - \frac{5}{6}\log(1-\kappa) - \frac{15}{6}\log(\kappa) - \frac{2}{3}$$

The polylogarithms, $Li_j(\kappa)$, and Spence functions, $S_{1,2}(\kappa)$ are defined in the first paper of Ref. 4.

The form of $\sigma_{obs}(s)$ given in Ref. 14 is given below in the notation of this paper.

$$\sigma_{obs}(s) = \sigma_Z(1+\delta_1)\frac{\Gamma_Z^2}{\Gamma_Z^2 + M_Z^2}$$
$$\left[\frac{s}{M_Z^2}a^{\beta-2}\Phi(\cos\theta,\beta) - a^{\beta-1}\frac{\beta}{1+\beta}\Phi(\cos\theta,1+\beta)\right] \qquad (46)$$
$$- \sigma_Z\beta\frac{\Gamma_Z}{\sqrt{s}}\left[\tan^{-1}\frac{2M_Z}{\Gamma_Z} - \tan^{-1}\frac{2(M_Z-\sqrt{s})}{\Gamma_Z}\right]$$

In this equation we make the approximation $\delta_1 \approx \frac{3}{4}\beta$. The quantities a, $\cos\theta$, and $\Phi(\cos\theta,\beta)$ are defined as follows:

$$a^2 = \frac{M_Z^2(s/M_Z^2-1)^2 + \Gamma_Z^2(s/M_Z^2)^2}{\Gamma_Z^2 + M_Z^2} \qquad (47)$$

$$\cos\theta = -\frac{M_Z^2(s/M_Z^2-1) + \Gamma_Z^2(s/M_Z^2)}{a(\Gamma_Z^2 + M_Z^2)} \qquad (48)$$

$$\Phi(\cos\theta,\beta) = \frac{\pi\beta\sin((1-\beta)\theta)}{\sin\pi\beta\sin\theta} \qquad (49)$$

The following four equations give $\sigma_{obs}(s)$ for four different levels of radiative correction, corresponding to the four curves in Fig. 3.

Pure first order:

$$\sigma_{obs}(s) = \sigma_0(s)(1+\delta_1+\beta\log\kappa_0) + \int_{\kappa_0}^{1} \beta(\frac{1}{\kappa}-1+\frac{\kappa}{2})\sigma_0(s')d\kappa \quad . \tag{50}$$

As noted earlier, $s' = s(1-\kappa)$. The Born cross section, $\sigma_0(s)$, is given in Eq. (1).

First order with exponentiation:

$$\sigma_{obs}(s) = \sigma_0(s)(1+\delta_1)\kappa_0^{\beta} + \int_{\kappa_0}^{1} \beta(\kappa^{\beta-1}(1+\delta_1)-1+\frac{\kappa}{2})\sigma_0(s')d\kappa \quad . \tag{51}$$

Pure second order:

$$\begin{aligned}\sigma_{obs}(s) = {} & \sigma_0(s)(1+\delta_1+\delta_2+\beta\log\kappa_0+\delta_1\beta\log\kappa_0+\frac{1}{2}\beta^2\log^2\kappa_0) \\ & + \int_{\kappa_0}^{1} \sigma_0(s')\left[\beta\left(\frac{1}{\kappa}-1+\frac{\kappa}{2}\right)(1+\delta_1+\beta\log(\kappa))\right. \\ & \left. +(\frac{\alpha}{\pi})^2\left(\frac{1+(1-\kappa)^2}{\kappa}A(\kappa)+(2-\kappa)B(\kappa)+(1-\kappa)C(\kappa)\right)\right]d\kappa\end{aligned} \tag{52}$$

Second order with exponentiation:

$$\begin{aligned}\sigma_{obs}(s) = {} & \sigma_0(s)(1+\delta_1+\delta_2)\kappa_0^{\beta} \\ & + \int_{\kappa_0}^{1} \sigma_0(s')\left[\beta\left(\kappa^{\beta-1}(1+\delta_1+\delta_2)-1+\frac{\kappa}{2}\right)\right. \\ & \left. +(\frac{\alpha}{\pi})^2\left(\frac{1+(1-\kappa)^2}{\kappa}A(\kappa)+(2-\kappa)B(\kappa)+(1-\kappa)C(\kappa)\right)\right]d\kappa\end{aligned} \tag{53}$$

Finally, we give the expression for the $f(\kappa, s)$ in Eq. (6) as given by the structure function analysis of Ref. 3.

$$
\begin{aligned}
f(\kappa,s) = {} & \beta\kappa^{\beta-1}\left[1+\delta_1-\frac{\beta^2}{24}\left(\frac{1}{3}\log\frac{s}{m_e^2}+2\pi^2-\frac{37}{4}\right)\right]-\beta\left(1-\frac{1}{2}\kappa\right) \\
& +\frac{1}{8}\beta^2\left[-4(2-\kappa)\log\kappa-\frac{(1+3(1-\kappa)^2)}{\kappa}\log(1-\kappa)-6+\kappa\right] \\
& +\left(\frac{\alpha}{\pi}\right)^2\left\{\frac{1}{6\kappa}\left(\kappa-\frac{4m_e}{\sqrt{s}}\right)^{\beta}\left(\log\left(\frac{s\kappa^2}{m_e^2}\right)-\frac{5}{3}\right)^2\right. \\
& \times\left(2-2\kappa+\kappa^2+\frac{1}{3}\beta\left(\log\left(\frac{s\kappa^2}{m_e^2}\right)-\frac{5}{3}\right)\right) \\
& \left.+\frac{1}{2}\log^2\frac{s}{m_e^2}\left[\frac{2(1-(1-\kappa)^3)}{3(1-\kappa)}+(2-\kappa)\log(1-\kappa)+\frac{1}{2}\kappa\right]\right\} \\
& \times\theta\left(\kappa-\frac{4m_e}{\sqrt{s}}\right)
\end{aligned}
\tag{54}
$$

REFERENCES

1. Mark II Coll. and SLC Final Focus Group, SLAC–SLC–PROP–2 (1986).
2. Mark II Proposal for SLC, SLAC–PUB–3561.
3. E. A. Kuraev and V. S. Fadin, Sov. J. Nucl. Phys. **41(3)**, 466 (1985).
4. R. Barbieri, J. A. Mignaco and E. Remiddi, Nuovo Cim. **11A**, 824 (1972); G. J. H. Burgers, Phys. Lett. **164B**, 167 (1985).
5. T. Kinoshita, J. Math. Phys. **3**, 650 (1962); T. D. Lee and M. Nauenberg, Phys. Rev. **133B**, 1549 (1964).
6. See, for example, B. W. Lynn, M. E. Peskin and R. G. Stuart, SLAC–PUB–3725.
7. The "virtual" term contains contributions from both vertex diagrams *and* bremsstrahlung diagrams: in the infrared limit, the two diagrams are not distinguishable. We use the term "virtual" to refer to corrections which have no dependence on measurable photon momenta, and "real" to refer to those corrections which do have such a dependence. Thus δ_1 is a correction arising from virtual photons, and $\beta \log k_{max}/E$ is a correction arising from real, radiated photons.
8. J. Alexander *et al.,* SLAC–REP–306, p. 45.
9. F. A. Berends, G. J. H. Burgers and W. L. Van Neerven, Phys. Lett. **185B**, 395 (1987).
10. G. Altarelli and G. Martinelli, CERN/EP 86–02, p. 47.
11. O. Nicrosini and L. Trentadue, UPRF–86–132.
12. The δ_2 given in the text [Eq. (16)] is from Ref. 11, where real and virtual pairs are consistently ignored throughout the paper. Reference 9 includes virtual pairs but not real pairs, thereby generating a term proportional to $\alpha^2 \log^3(\frac{s}{m_e^2})$ as well as affecting the coefficients of the terms proportional to

$\alpha^2 \log^n(\frac{s}{m_e^2})$, where $n = 0, 1, 2$. Reference 3 consistently adds real and virtual pairs, resulting in a cancellation of the $\alpha^2 \log^3(\frac{s}{m_e^2})$ term in $D_{eee}(x, s)$.

13. D. R. Yennie, S. C. Frautschi and H. Suura, Ann. of Phys. **13,** 379 (1961).

14. R. N. Cahn, Phys. Rev. D., to be published. The first analytic formula for a narrow resonance was derived in M. Greco *et al.,* Phys. Lett. **56B,** 367 (1975).

15. L. N. Lipatov, Sov. J. Nucl. Phys. **20,** 94 (1975).

16. L. N. Lipatov and V. N. Gribov, Sov. J. Nucl. Phys. **15,** 438 (1972).

17. J. Kogut and L. Susskind, Phys. Rep. **8,** 75 (1973).

18. G. Altarelli and G. Parisi, Nucl. Phys. B **126,** 298 (1977).

19. F. A. Berends, R. P. Kleiss and S. Jadach, Nucl. Phys. B **202,** 63 (1982); Comp. Phys. Comm. **29,** 185 (1983).

20. Y. L. Dokshitser, D. I. Dyakonov and S. I. Troian, Phys. Rep. **58,** 269 (1980).

21. J. D. Jackson and D. L. Scharre, Nucl. Instrum. Methods **128,** 13 (1975). Their formula was originally derived by Y. S. Tsai, SLAC–PUB–1515.

22. B. W. Lynn, G. Penso and C. Verzegnassi, Phys. Rev. D **35,** 42 (1987); F. Jegerlehner, Z. Phys. C **32,** 195 (1986).

23. M. Greco, CERN/EP 86–02, p. 186.

24. A. M. Boyarski *et al.,* Phys. Rev. Lett. **34,** 1357 (1975).

25. Particle Data Book, Phys. Lett. **170B** (1986).

TABLE CAPTIONS

1. Accuracy of various levels of approximation on the fit parameters M_Z, Γ_Z, and σ_Z relative to the exponentiated second order calculation of Ref. 9. δQ, with $Q = M_Z$, Γ_Z, or σ_Z, is defined as $Q - Q_9$, where Q_9 is from Ref. 9.

2. Comparison of cross section values, stated as a percent deviation from the cross section of Ref. 9.

3. Results of comparing different calculations for extraction of M_Z, Γ_Z, and σ_Z given data generated by Ref. 9. The differences are defined as in Table 1.

Table 1

Fitting Function	δM_Z (MeV/c^2)	$\delta\Gamma_Z$ (MeV)	$\frac{\delta\sigma_Z}{\sigma_Z}$ (%)
1st order	−121	−152	5.63
Exp. 1st order	1	2	−0.54
2nd order (Ref. 9)	14	12	−0.11

Table 2

Fitting Function	$\frac{\delta\sigma_Z}{\sigma_Z}$ (%) at $\sqrt{s}$ (GeV) =			
	91	93	95	97
Berends, *et al.* (Ref. 9)	–	–	–	–
Jackson and Scharre (Ref. 21)	4.56	4.31	−0.098	−3.07
Cahn (Ref. 14)	−0.670	−0.034	−0.156	−0.681
Trentadue and Nicrosini (Ref. 11)	0.019	0.025	−0.051	−0.203
Fadin and Kuraev (Ref. 3)	< 0.001	0.003	0.017	0.014

Table 3

Fitting Function	δM_Z (MeV/c^2)	$\delta\Gamma_Z$ (MeV)	$\frac{\delta\sigma_Z}{\sigma_Z}$ (%)
Berends, *et al.* (Ref. 9)	–	–	–
Jackson and Scharre (Ref. 21)	35	69	−4.45
Cahn (Ref. 14)	−0.2	8.9	−0.01
Trentadue and Nicrosini (Ref. 11)	1.1	1.4	−0.84
Fadin and Kuraev (Ref. 3)	< 0.1	0.2	−0.01

FIGURE CAPTIONS

1. Lowest order diagrams for the process $e^+e^- \to f\bar{f}$.

2. Diagrams for the first order correction. Note that the loop in (d) includes all fermions. There are four $\gamma - Z^0$ box diagrams represented by (h), and two $\gamma - \gamma$ box diagrams represented by (i).

3. The Z^0 line shape with various levels of radiative corrections. Dot-dash curve: first order; dashed curve: first order with exponentiation; dotted curve: second order; solid curve: second order with exponentiation.

4. An electron-photon cascade of the sort described by structure functions.

5. Diagrams involving real and virtual pairs in the initial state. Emission of real pairs is depicted in diagrams (a) and (b), while (c) and (d) are the analgous processes involving virtual pairs.

6. A lowest order virtual correction incorporated in δ_1.

7. Photon bremsstrahlung down to a resonance. In this case, the virtual correction has a relatively large effect on the overall cross section.

8. Forward-backward asymmetry as a function of $\sqrt{s}$ for levels of correction. Dotted curve: lowest order; dashed curve: first order; solid curve: second order with exponentiation.

9. The J/ψ resonance shape from Ref. 24. The fit has been obtained using one of the Monte Carlos described in the text.

10. The function $f'(k/E, s)$ as measured in Ref. 24.

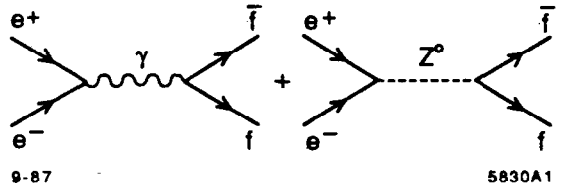

Fig. 1

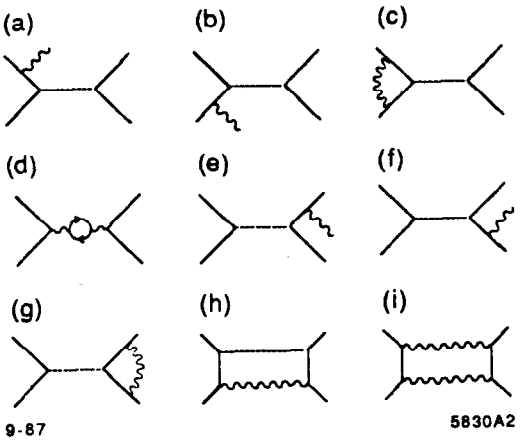

Fig. 2

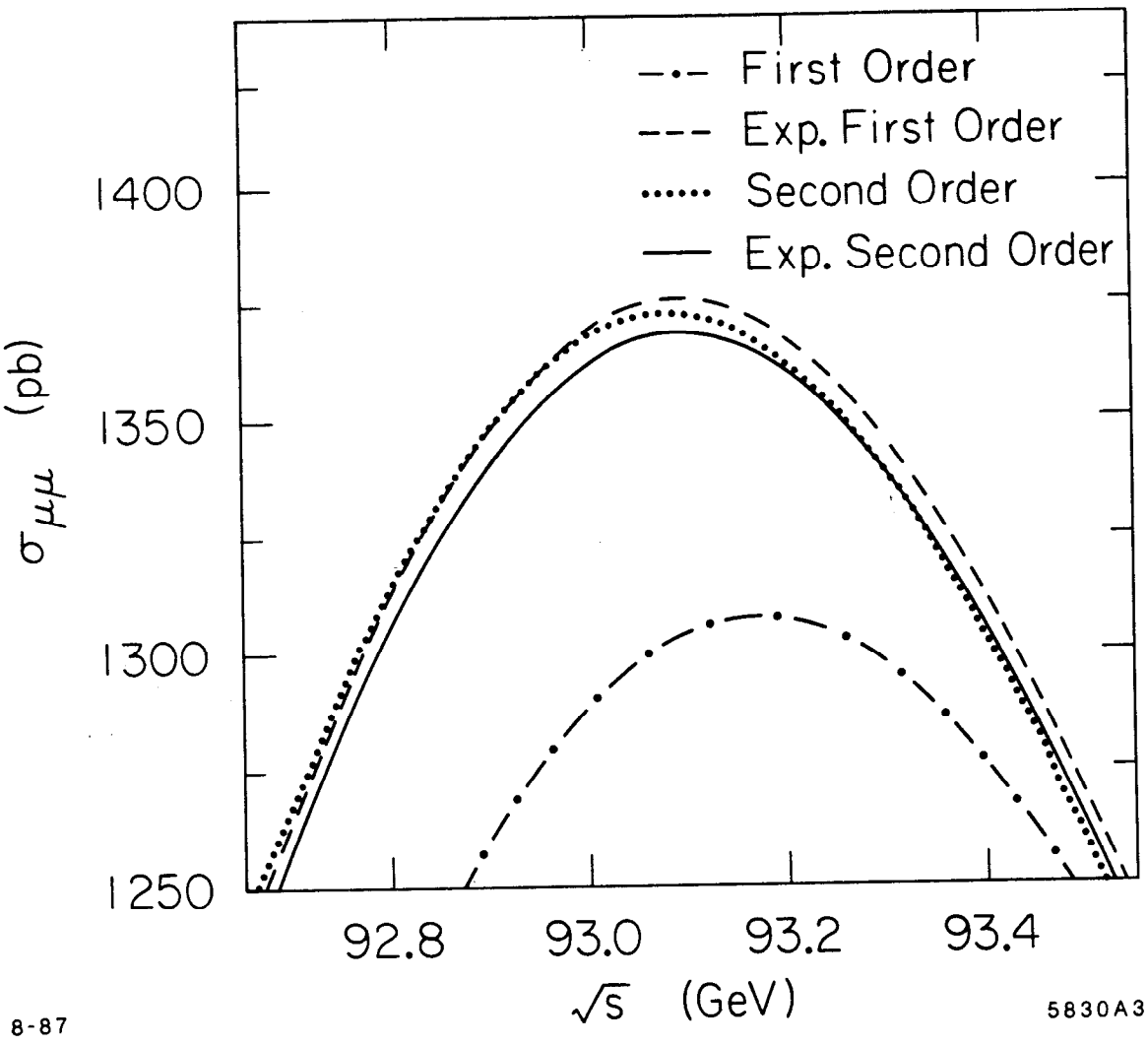
First Order
Exp. First Order
Second Order
Exp. Second Order
1400
1350
1300
1250
$\sigma_{\mu\mu}$ (pb)
92.8
93.0
93.2
93.4
$\sqrt{s}$ (GeV)
8-87
5830A3

Fig. 3

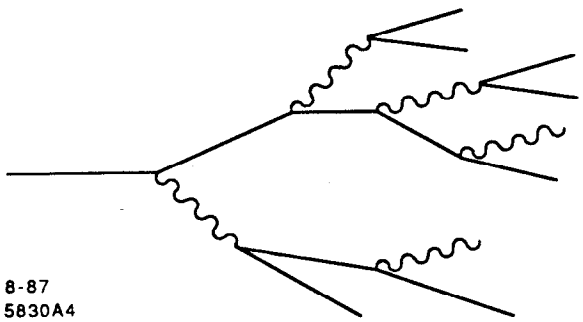

8-87
5830A4

Fig. 4

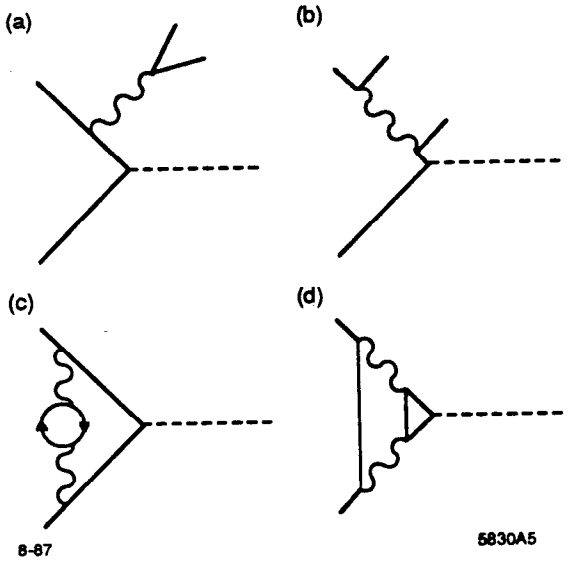

Fig. 5

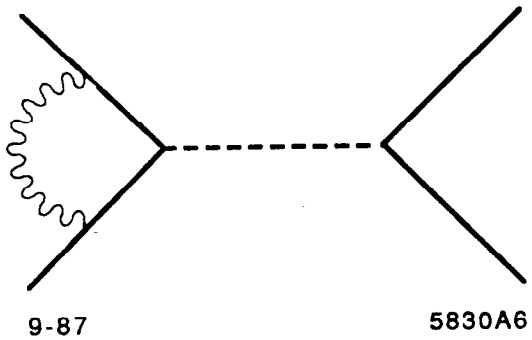

Fig. 6

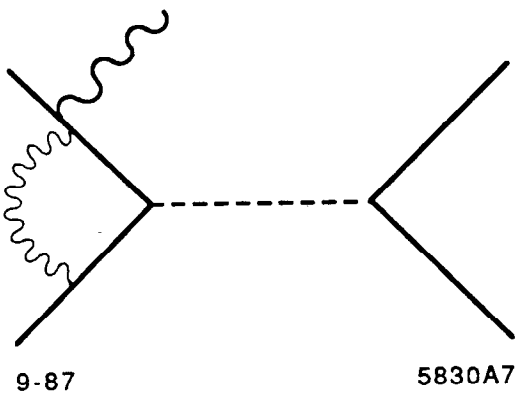

Fig. 7

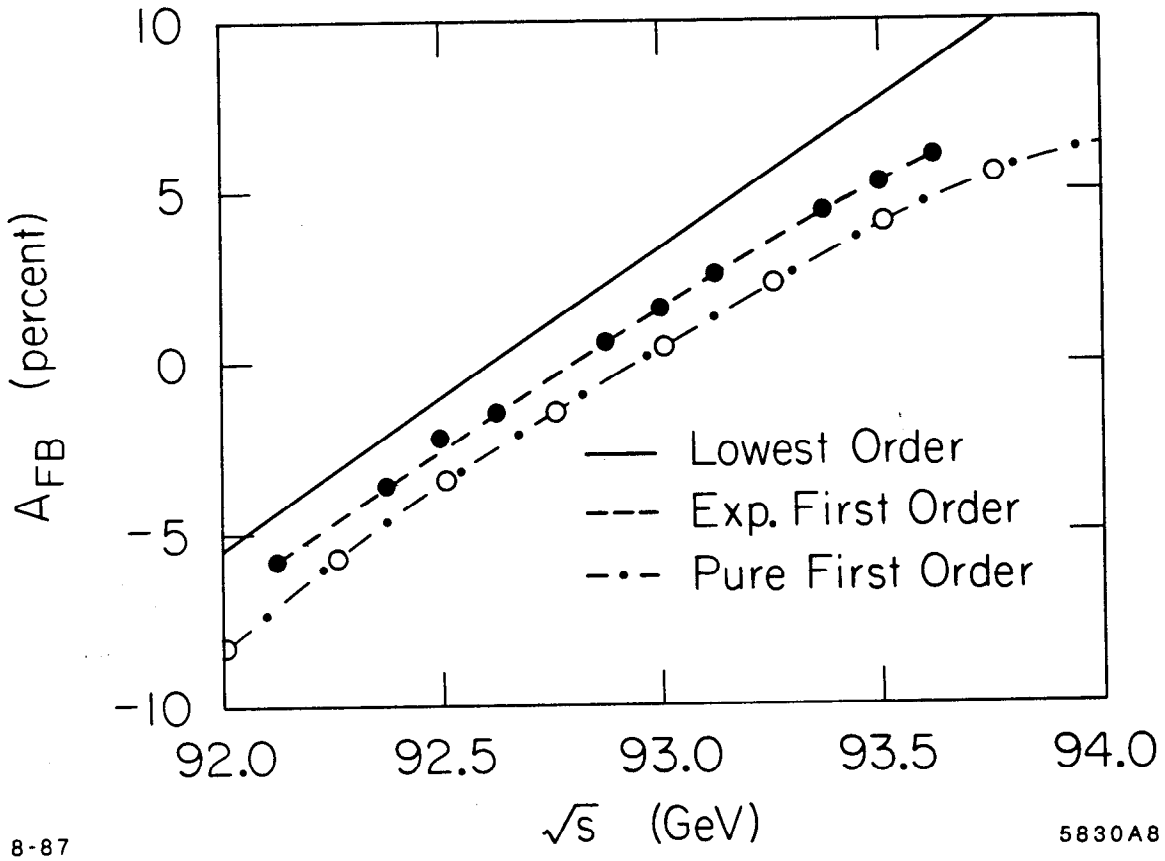
10
5
0
−5
−10
92.0
92.5
93.0
93.5
94.0
A_{FB} (percent)
$\sqrt{s}$ (GeV)
Lowest Order
Exp. First Order
Pure First Order
8-87
5830A8

Fig. 8

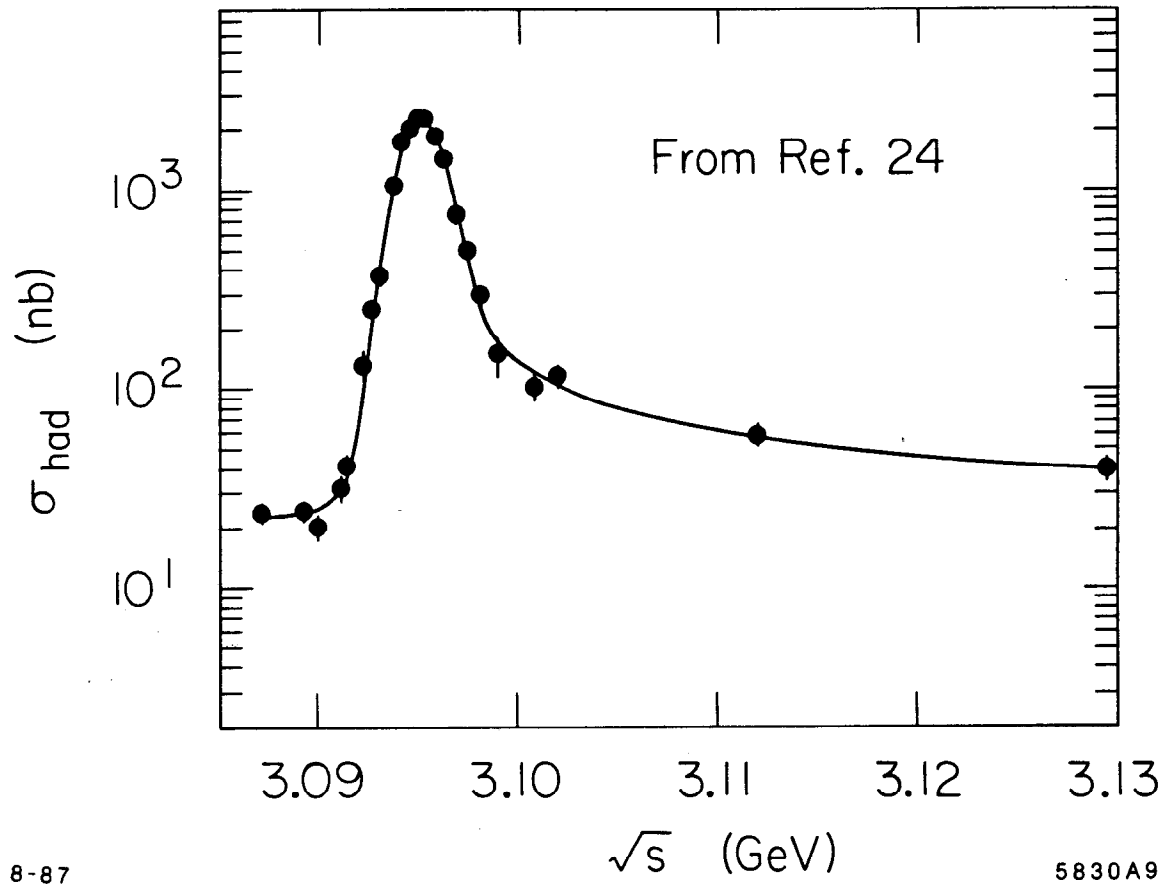
From Ref. 24
10^3
10^2
10^1
σ_{had} (nb)
3.09
3.10
3.11
3.12
3.13
$\sqrt{s}$ (GeV)
8-87
5830A9

Fig. 9

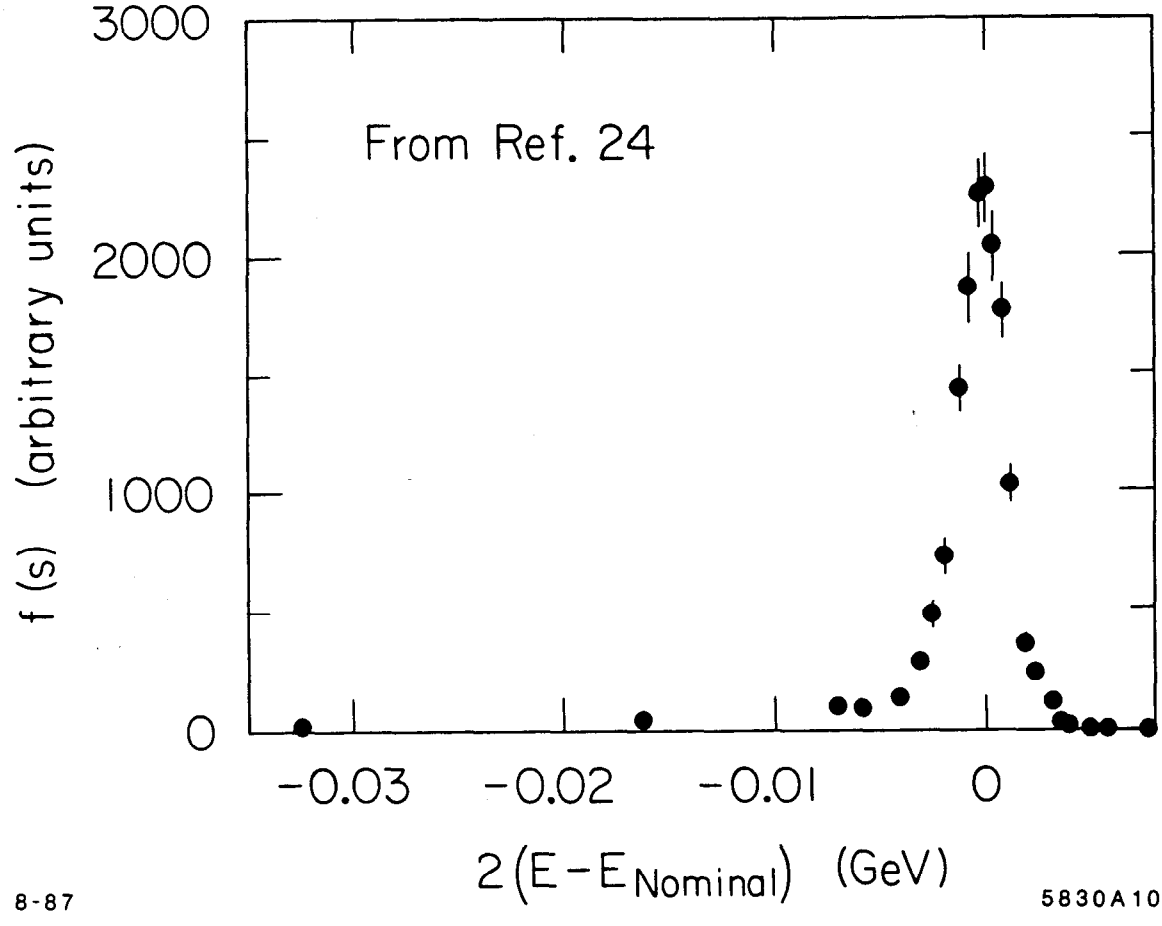
From Ref. 24
3000
2000
1000
0
f (s) (arbitrary units)
-0.03
-0.02
-0.01
0
2(E-E Nominal) (GeV)
8-87
5830A10

Fig. 10